DOI: 10.1143/JJAP.51.024301

A Subthreshold Current Model of Fully-Depleted Silicon-on-Insulator Metal–Oxide–Semiconductor Field Effect Transistors with Vertical Gaussian Profile

Guohe Zhang, Kebin Chen, and Feng Liang*

School of Electronic and Information Engineering, Xi'an Jiaotong University, Shaanxi 710049, China

Received September 14, 2011; accepted November 21, 2011; published online January 23, 2012

A subthreshold current of fully-depleted (FD) silicon-on-insulator (SOI) metal–oxide–semiconductor field effect transistors (MOSFETs) with vertical Gaussian profile is presented in the paper. The model is based on analytical approximated solution of two-dimensional Poissons' equation and Boltzmann transport equation. The front and the back channel currents are effectively derived using a novel inversion layer model and the boundary conditions which take the nonuniform doping into account. The results are matched well with the numerical simulation results obtained by Sentaurus Technology Computer-Aided Design (TCAD). The model is believed to provide a deep physical insight and understanding of FD-SOI MOSFETs with a non-uniform doping profile operating in the subthreshold regime. © 2012 The Japan Society of Applied Physics

1. Introduction

With the size scaling down, metal–oxide–semiconductor field effect transistors (MOSFETs) operated in subthreshold region have played an ever increasingly important role in low power consumption and high energy efficiency applications.[1,2] Fully-depleted (FD) silicon-on-insulator (SOI) MOSFETs have attracted considerable attention due to their superior short-channel immunity and ideal subthreshold characteristics. In order to perform a robust design and get insight to the device physics, compact models which include the relation between subthreshold current and device parameters are required. A number of theoretical subthreshold current models for SOI MOSFETs[3–6] have been developed based on the classical physics-based formulations. Both the diffusion and the drift components of subthreshold current, as well as the charge sharing effect and the drain-induced barrier lowering effect, should be considered especially for deep submicron SOI MOSFETs. Analytical two-dimensional (2D) approximation of Poisson's equation solution, which describes the potential distribution in the SOI film, can effectively reflect the charge coupling between the front- and back-gates in the FD SOI MOSFETs.[7)]

One of the fundamental assumptions in most references is that the SOI film doping concentration is uniform. However, in practice, it is not easy to keep the channel uniformly doped throughout the region as the precise control over doping is impossible. It may well be that the transistor channel doping profile becomes closer to Gaussian profile in nature due to many ion implantation stages required during the fabrication process.[7–11] Furthermore, after some of the fabrication stages like retrograde channel doping in the vertical channel engineering,[12–14] the original implant gets altered after thermal annealing and the annealed profile can be nearly assumed uniform in the lateral direction and nonuniform in the vertical direction. The Gaussian distribution is the most general doping profile from which a number of different doping profiles can be derived by varying the projected range, R_p, and the projected deviation, σ_p of the Gaussian function.

In this paper, an analytical subthreshold current is developed for FD SOI MOSFETs with vertical Gaussian profile based on the analytical solving of the 2D Poisson's equations. During the calculation of inversion layer thickness in the subthreshold regime, the total number of electron corresponding to the non-uniform doping profile is considered. The model results are compared with the simulation results obtained by the Sentaurus Technology Computer-Aided Design (TCAD) device simulator.

*E-mail address: fengliang@mail.xjtu.edu.cn

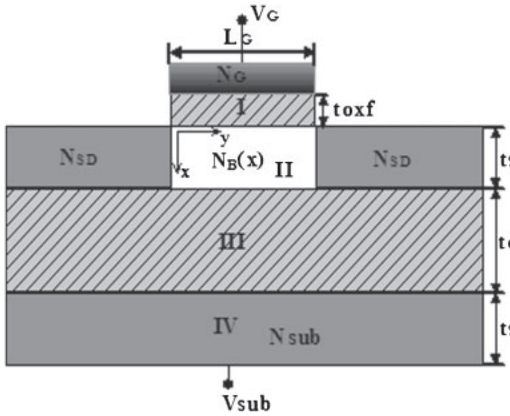

Fig. 1. Cross section of simulated structure.

2. Model Derivations

The device structure under consideration is shown in Fig. 1. t_{si} is the silicon film thickness, $N_B(x)$ is the variable doping concentration in p-type SOI film, t_{oxf} is the forward oxide thickness and t_{oxb} is the buried-oxide thickness, t_{sub} is substrate thickness. The doping profile in the vertical direction of the channel, $N_B(x)$, is assumed to be a Gaussian function

$$N_B(x) = N_p \exp\left[-\frac{1}{2}\left(\frac{x - R_p}{\sigma_p}\right)^2\right] \quad (1)$$

where N_p is the peak concentration of the vertical Gaussian doping profile.

The device characteristics were simulated using the 2D numerical device simulator Sentaurus TCAD. As the subthreshold current is too small, the logarithmic I_{DS}–V_{GS} curve (at some small V_{DS}) is required.

As we derived in ref. 7, the back surface potential ϕ_b and the front surface potential ϕ_s have been obtained through solving the 2D Poisson's equations:

 © 2012 The Japan Society of Applied Physics

$$\phi_b(y) = V'_{GS} + V_1 + \frac{\xi_S \sinh[(L_G - y)/\lambda_b] + \xi_D \sinh(y/\lambda_b)}{\sinh(L_G/\lambda_b)}, \tag{2}$$

$$\phi_s(y) = V'_{GS} + V_2 + \frac{\eta_S \sinh[(L_G - y)/\lambda_f] + \eta_D \sinh(y/\lambda_f)}{\sinh(L_G/\lambda_f)}, \tag{3}$$

$$V_1 = -\frac{(\gamma t_{oxf} + t_{si})(V'_{GS} - V'_{sub})}{(\gamma t_{oxf} + \gamma t_{oxb} + t_{si})} - \frac{\gamma\sigma_p^2 t_{oxb}(\gamma t_{oxf} - D)[\exp(-A^2) - \exp(-B^2)]}{(D + R_p)(\gamma t_{oxf} + \gamma t_{oxb} + t_{si})}\frac{qN_p}{\varepsilon_{si}}, \tag{4}$$

$$V_2 = -\frac{\gamma t_{oxf}(V'_{GS} - V'_{sub})}{\gamma t_{oxf} + \gamma t_{oxb} + t_{si}} - \frac{\gamma\sigma_p^2 t_{oxf}(\gamma t_{oxb} + t_{si} + D)[\exp(-A^2) - \exp(-B^2)]}{(D + R_p)(\gamma t_{oxf} + \gamma t_{oxb} + t_{si})}\frac{qN_p}{\varepsilon_{si}}, \tag{5}$$

where

$$\gamma = \frac{\varepsilon_{si}}{\varepsilon_{ox}},$$
$$V'_{GS} = V_{GS} - V_{FB},$$
$$V'_{sub} = V_{sub} - V_{FBsub},$$
$$A = \frac{t_{si} - R_p}{\sqrt{2}\sigma_p},$$
$$B = -\frac{R_p}{\sqrt{2}\sigma},$$
$$D = \frac{\sqrt{2}\sigma_p[\exp(-A^2) - \exp(-B^2)]}{\sqrt{\pi}[\mathrm{erf}(A) - \mathrm{erf}(B)]} - R_p.$$

ε_{si} and ε_{ox} are respectively the dielectric permittivity of silicon and SiO_2. V_{FB} is the surface flat-band voltage, and V_{FBsub} is the flat-band voltage between the back channel and the substrate. λ_b and λ_f are the characteristic lengths associated with ϕ_b and ϕ_s and can be written as

$$\lambda_b^2 = \frac{\gamma t_{oxb}(\gamma t_{oxf} - D)}{2(D + R_p)(\gamma t_{oxf} + \gamma t_{oxb} + t_{si})} \cdot \{2\sigma_p^2[1 - \exp(A^2 - B^2)] + (D + R_p)t_{oxb}\}, \tag{6}$$

$$\lambda_f^2 = \frac{\gamma\{t_{oxf}\sigma_p^2(\gamma t_{oxf} + \gamma t_{oxb} + t_{si})[2\gamma\lambda_b^2 t_{oxb} + (t_{si} + D)(2\lambda_b^2 - t_{oxb}^2)][\exp(B^2 - A^2) - 1] + \lambda_b^2 t_{oxb}^3(\gamma t_{oxf} - D)(D + R_p)\}}{(D + R_p)(\gamma t_{oxf} + \gamma t_{oxb} + t_{si})[2\gamma\lambda_b^2 t_{oxb} + (t_{si} + D)(2\lambda_b^2 - t_{oxb}^2)]}. \tag{7}$$

The position where potential is minimum in the surface can be derived as $d\phi/dy = 0$. According to eqs. (2) and (3), we can obtain

$$y_m(\phi_b) = \frac{\lambda_b}{2}\ln\left[\frac{\xi_S \exp(L_G/\lambda_b) - \xi_D}{\xi_D - \xi_S \exp(-L_G/\lambda_b)}\right], \tag{8}$$

$$y_m(\phi_s) = \frac{\lambda_f}{2}\ln\left[\frac{\eta_S \exp(L_G/\lambda_f) - \eta_D}{\eta_D - \eta_S \exp(-L_G/\lambda_f)}\right]. \tag{9}$$

Substituting eqs. (8) and (9) into eqs. (2) and (3), respectively, the minimum potential associated with back surface $\phi_b(y_m)$ and front surface $\phi_s(y_m)$ can be obtained. According to drift-diffusion approximation,[4] the subthreshold current density model using the Boltzmann transport equation can be expressed as

$$J_n = -nq\mu_n\frac{d\phi_n}{dy} = -n_i q\mu_n \exp\left(\frac{\phi - \phi_n}{\phi_t}\right)\cdot\frac{d\phi_n}{dy}, \tag{10}$$

where μ_n is the electron mobility, ϕ_n is the electron quasi-Fermi level, ϕ is the electrostatic potential and $\phi_t = kT/q$. Considering the boundary condition, the quasi-Fermi level of back surface must satisfy

$$\phi_{nb}(0) = \phi_{Bbeff} = \phi_t \ln\left(\frac{N_{Bbeff}}{n_i}\right), \tag{11}$$

$$\phi_{nb}(L_G) = \phi_{Bb} + V_{DS} = \phi_t \ln\left(\frac{N_{Bb}}{n_i}\right) + V_{DS}, \tag{12}$$

where N_{Bb} is the back surface doping concentration. As the component of subthreshold current in the back surface is not dominant, the above approximate boundary condition is acceptable. But in the front surface, it must be too coarse and a more accurate boundary condition should be considered.

$$\phi_{ns}(0) = \phi_{Bseff} = \phi_t \ln\left(\frac{N_{Bseff}}{n_i}\right), \tag{13}$$

$$\phi_{ns}(L_G) = \phi_{Bseff} + V_{DS} = \phi_t \ln\left(\frac{N_{Bseff}}{n_i}\right) + V_{DS}, \tag{14}$$

where

$$N_{Bseff} = \int_0^{x_{min}} N_B(x)dx = \sqrt{2}\sigma_p N_p\left[\mathrm{erf}\left(\frac{x_{min} - R_p}{\sqrt{2}\sigma_p}\right) - \mathrm{erf}(B)\right],$$

and x_{min} is defined as the position of the minimum potential along the x-axis. According to ref. 7, we can obtain

$$\mathrm{erf}\left(\frac{x_{min} - R_p}{\sqrt{2}\sigma_p}\right) = -\frac{(V'_{GS} - \phi_s)\,\mathrm{erf}(A) - t_{oxf}E_b\,\mathrm{erf}(B)}{V'_{GS} - \phi_s - t_{oxf}E_b} = H. \tag{15}$$

E_b is the electric field at the back channel in buried-oxide layer side. Using the properties of the error function, the value of x_{min} can be derived from eq. (15) through five-stage Taylor's series approximation:

$$x_{min} = \sqrt{2}\sigma_p\left(H + \pi\frac{H^3}{480} + 7\pi^2\frac{H^5}{480} + 127\pi^3\frac{H^7}{40320} + 4369\pi^4\frac{H^9}{5806080}\right) + R_p. \tag{16}$$

Substituting eqs. (13) and (14) into eq. (10) and integrating the resulting equation from source to drain and assuming the front surface lateral current density J_{ns} is constant, we can obtain

© 2012 The Japan Society of Applied Physics

$$J_{\rm ns} = -q\mu_{\rm n}\phi_{\rm t}n_{\rm i}\exp\left(-\frac{\phi_{\rm Bs}}{\phi_{\rm t}}\right) \times \left[1-\exp\left(-\frac{V_{\rm DS}}{\phi_{\rm t}}\right)\right] \Bigg/ \int_0^{L_{\rm G}} \exp\left(-\frac{\phi}{\phi_{\rm t}}\right)dy. \quad (17)$$

In the long-channel case, the surface potential is constant and the integral in the denominator of eq. (17) becomes $L\exp(-\phi_{\rm s}/\phi_{\rm t})$, but for short-channel devices, it will result in higher drain current. To accomplish the integral in eq. (17), we give an approximate result as

$$\int_0^{L_{\rm G}} \exp\left(-\frac{\phi_{\rm s}}{\phi_{\rm t}}\right)dy = \exp\left[-\frac{\phi_{\rm s}(y_{\rm m})-0.5\phi_{\rm t}}{\phi_{\rm t}}\right]L_{\rm eff}, \quad (18)$$

where $L_{\rm eff}$ is the effective front channel length. The electron concentration depends exponentially on the electrostatic potential, the current flow can be considered to have a depth at which the potential decreases by $\phi_{\rm t}$.[15] So we use the middle potential of the inversion layer to replace the surface potential here.

$L_{\rm eff}$ is the effective channel length which can be expressed as[6]

$$L_{\rm eff} = L_{\rm G} - L_{\rm S} - L_{\rm D}. \quad (19)$$

$L_{\rm S}$ and $L_{\rm D}$ are the positions where the charge is controlled by the source or the drain, which can be written as

$$L_{\rm S} = \frac{[V_{\rm bis} - \phi_{\rm s}(y_{\rm m})]}{E_{\rm eff1}}, \quad L_{\rm D} = \frac{[V_{\rm bis} + V_{\rm DS} - \phi_{\rm s}(y_{\rm m})]}{E_{\rm eff2}}. \quad (20)$$

$E_{\rm eff1}$ and $E_{\rm eff2}$ are the effective lateral electric fields at the front interface between channel and the source, or the drain, which can be defined as

$$E_{\rm eff1} = \sqrt{\frac{qN_{\rm Bseff}[V_{\rm bis}-\phi_{\rm s}(y_{\rm m})]}{2\varepsilon_{\rm si}}} + \frac{f_\alpha}{\gamma}\frac{V'_{\rm GS}-\phi_{\rm s}(y_{\rm m})}{t_{\rm oxf}} + \frac{f_\beta}{\gamma}\frac{V_{\rm bis}-V'_{\rm GS}}{t_{\rm oxf}}, \quad (21)$$

$$E_{\rm eff2} = \sqrt{\frac{qN_{\rm Bseff}[V_{\rm bis}+V_{\rm DS}-\phi_{\rm s}(y_{\rm m})]}{2\varepsilon_{\rm si}}} + \frac{f_\alpha}{\gamma}\frac{V'_{\rm GS}+V_{\rm DS}-\phi_{\rm s}(y_{\rm m})}{t_{\rm oxf}} + \frac{f_\beta}{\gamma}\frac{V_{\rm bis}-V'_{\rm GS}}{t_{\rm oxf}}, \quad (22)$$

where

$$V_{\rm bis} = \phi_{\rm t}\ln\frac{N_{\rm Bs}N_{\rm SD}}{n_{\rm i}^2},$$

$N_{\rm SD}$ is the doping concentration of source and drain. In calculating these electric fields, the first term is due to the depletion charge of the abrupt p–n junction, whereas the second and the third terms are due to the fringing fields with fitting parameters f_α and f_β estimated as in ref. 6. The channel depth for current flow can be given as[16]

$$y_{\rm s} = \frac{N_{\rm is}}{n_{\rm s}}, \quad (23)$$

where $N_{\rm is}$ is the total number of electron in the inversion layer and $n_{\rm s}$ is the electron concentration in the front surface:

$$n_{\rm s} = n_{\rm i}\exp\left[\frac{\phi_{\rm s}(y_{\rm m})-\phi_{\rm Bs}}{\phi_{\rm t}}\right]. \quad (24)$$

When neglecting the band bending because of ionized acceptors, the Poisson's equation for inversion layer is expressed as

$$\frac{d^2\phi}{dx^2} = \frac{q}{\varepsilon_{\rm si}}n, \quad (25)$$

where n is the electron concentration. Multiplying the left- and right-hand sides of eq. (23) by $d\phi/dx$ and integrating from some reference position $x_{\rm ref}$ to x gives

$$\frac{1}{2}\left(\frac{d\phi}{dx}\right)^2 - \frac{1}{2}\left(\frac{d\phi}{dx}\right)^2_{\rm ref} = \frac{kT}{\varepsilon_{\rm si}}(n-n_{\rm ref}). \quad (26)$$

Using electromagnetic field theory, we obtain

$$\frac{dE}{dx} = \frac{q}{\varepsilon_{\rm si}}n. \quad (27)$$

Integrating eq. (25) from x to the position x min where the potential is minimum, we can get

$$E_{x_{\rm min}} - E(x) = \frac{q}{\varepsilon_{\rm si}}\left(\int_x^{x_{\rm min}} n_{\rm d}\,dx + \int_x^{x_{\rm min}} n\,dx\right), \quad (28)$$

where $n_{\rm d}$ is the concentration of ionized acceptors. As for electric potential, the $x_{\rm min}$ is a stationary point. Thus $E_{x_{\rm min}}$ is zero, and eq. (26) can be rewritten as

$$\frac{d\phi}{dx} = -E(x) = \frac{q}{\varepsilon_{\rm si}}\left(\int_x^{x_{\rm min}} n_{\rm d}\,dx + \int_x^{x_{\rm min}} n\,dx\right). \quad (29)$$

Substituting eq. (29) to eq. (26), and assuming that $x_{\rm ref}$ is so large that $\int_{x_{\rm ref}}^{x_{\rm min}} n\,dx = 0$ holds and noting that $N_{\rm d} = \int_x^{x_{\rm min}} n_{\rm d}\,dx = \int_x^{x_{\rm min}} N_{\rm B}(x)dx$ for FD SOI. So we can approximately obtain

$$N_{\rm is} = \int_0^{x_{\rm min}} n\,dx = \sqrt{N_{\rm deff}^2 + \frac{2\varepsilon_{\rm si}\phi_{\rm t}n_{\rm s}}{q}} - N_{\rm deff}, \quad (30)$$

where $N_{\rm deff}$ can be given by

$$N_{\rm deff} = \int_0^{x_{\rm min}} N_{\rm B}(x)dx = \sqrt{2}\sigma_{\rm p}N_{\rm p}\left[\mathrm{erf}\left(\frac{x_{\rm min}-R_{\rm p}}{\sqrt{2}\sigma_{\rm p}}\right) - \mathrm{erf}(B)\right]. \quad (31)$$

Thus the subthreshold current in the front surface can be expressed as

$$I_{\rm ns} = \frac{y_{\rm s}Wq\mu_{\rm n}\phi_{\rm t}n_{\rm i}\exp(-\phi_{\rm Bs}/\phi_{\rm t})[1-\exp(-V_{\rm DS}/\phi_{\rm t})]}{\exp\{-[\phi_{\rm s}(y_{\rm m})-\phi_{\rm t}/2]/\phi_{\rm t}\}L_{\rm eff}}, \quad (32)$$

where W is the channel width. In the same way, the back surface lateral current density can be expressed as

$$J_{\rm nb} = -q\mu_{\rm n}\phi_{\rm t}n_{\rm i}\exp\left(-\frac{\phi_{\rm Bb}}{\phi_{\rm t}}\right) \times \left[1-\exp\left(-\frac{V_{\rm DS}}{\phi_{\rm t}}\right)\right] \Bigg/ \int_0^{L_{\rm G}} \exp\left(-\frac{\phi_{\rm b}}{\phi_{\rm t}}\right)dy, \quad (33)$$

$$\int_0^{L_{\rm G}} \exp\left(-\frac{\phi_{\rm b}}{\phi_{\rm t}}\right)dy = \exp\left[-\frac{\phi_{\rm b}(y_{\rm m})-0.5\phi_{\rm t}}{\phi_{\rm t}}\right]L_{\rm effb}, \quad (34)$$

where $L_{\rm effb}$ is the effective length associated with front channel.

Note that the electron number in the inversion layer of back surface is much smaller than that in the front surface. Using eq. (23) to solve the inversion layer thickness of the back channel will be inaccuracy. In this case, the inversion depth of the back surface is modeled by

© 2012 The Japan Society of Applied Physics

$$y_{\mathrm{b}} = \frac{\phi_{\mathrm{s}}(y_{\mathrm{m}})}{\phi_{\mathrm{b}}(y_{\mathrm{m}})} y_{\mathrm{s}}. \tag{35}$$

Thus, the back channel substhreshold current is calculated as

$$I_{\mathrm{nb}} = \frac{y_{\mathrm{b}} W q \mu_{\mathrm{n}} \phi_{\mathrm{t}} n_{\mathrm{i}} \exp(-\phi_{\mathrm{Bb}}/\phi_{\mathrm{t}})[1 - \exp(-V_{\mathrm{DS}}/\phi_{\mathrm{t}})]}{\exp\{-[\phi_{\mathrm{b}}(y_{\mathrm{m}}) - \phi_{\mathrm{t}}/2]/\phi_{\mathrm{t}}\} L_{\mathrm{effb}}}. \tag{36}$$

Obviously, the total substhreshold current is

$$I = I_{\mathrm{nb}} + I_{\mathrm{ns}}. \tag{37}$$

3. Results and Discussion

In this section, the analytical results of the subthreshold current calculated from our model will be compared with the numerical results obtained by the device simulation software Sentaurus TCAD.

The subthreshold current variation as a function of gate voltage is shown in Figs. 2–4 for different doping concentrations. The current decreases with the increase of the total doping concentrations, because of the fact that higher doping concentration which increases the overall doping level of the channel makes the source-channel barrier rise and thereby the diffusion current which is dominant in subthreshold current is dropped. Further, higher doping concentration also makes inversion layer harder to form at the same gate voltage and hence the drift current in subthreshold current decreases as well. As doping concentration increases, the current density will drop according to eq. (17). The source–drain current values for different N_{p} (as shown in Fig. 2) at $V_{\mathrm{GS}} = 0.05\,\mathrm{V}$ are as follows: when $N_{\mathrm{p}} = 7 \times 10^{18}\,\mathrm{cm}^{-3}$, I_{DS} is about 1.1×10^{-11} A; when $N_{\mathrm{p}} = 5 \times 10^{18}\,\mathrm{cm}^{-3}$, I_{DS} is about 7.0×10^{-10} A; when $N_{\mathrm{p}} = 3 \times 10^{18}\,\mathrm{cm}^{-3}$, I_{DS} is about 5.3×10^{-8} A. Note that when N_{p} increases from 3×10^{18} to $7 \times 10^{18}\,\mathrm{cm}^{-3}$, the rising in subthreshold current is more than three orders in magnitude. Figure 3 shows the subthreshold current variation as a function of gate voltage for different standard deviation p of the Gaussian profile. The subthreshold current decreases with increasing the standard deviation. According to Fig. 3, I_{DS} values at $V_{\mathrm{GS}} = 0.05\,\mathrm{V}$ for $\sigma_{\mathrm{p}} = 5$ and 8 nm are about 5.4×10^{-8} and 2.9×10^{-8} A, respectively. In subthreshold regime, compared with $p = 8\,\mathrm{nm}$, the value of source–drain current at $\sigma_{\mathrm{p}} = 5\,\mathrm{nm}$ is about 2 times larger. In Fig. 4 a plot of the substhreshold current versus the front gate voltage is made for devices with different projected range values R_{p}. The front subthreshold current increases when the projected range deviates from the value of $x_{\min}/2$. At the bias of $V_{\mathrm{GS}} = 0.05\,\mathrm{V}$, the value of subthreshold current for $R_{\mathrm{p}} = 6\,\mathrm{nm}$ is about 5.3×10^{-8} A, which is less than the approximate current value 2.2×10^{-7} A at $R_{\mathrm{p}} = 2\,\mathrm{nm}$ by more than four times. Thus, doping concentration fluctuations can have an important impact on the current. It is obviously that considering the non-uniform doping concentration profile in short channel device will improve the accuracy of circuit design.

The dependence of subthreshold current on gate-oxide thickness t_{oxf} has been considered in Fig. 5. Note that the subthreshold current decreases with increased t_{oxf}. The increase of the gate-oxide thickness can give rise to the decreasing of the surface electric fields which reduce the controllability of the gate voltage. In other words, for the same gate voltage the device with thinker gate-oxide has less inversion charges in the surface.

Figure 6 shows the subthreshold current variations as a function of gate voltage for different substrate voltage. We

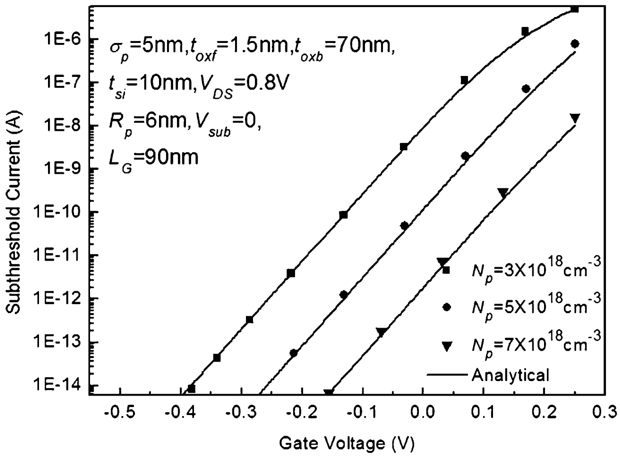

Fig. 2. Subthreshold current versus gate voltage for different N_{p}.

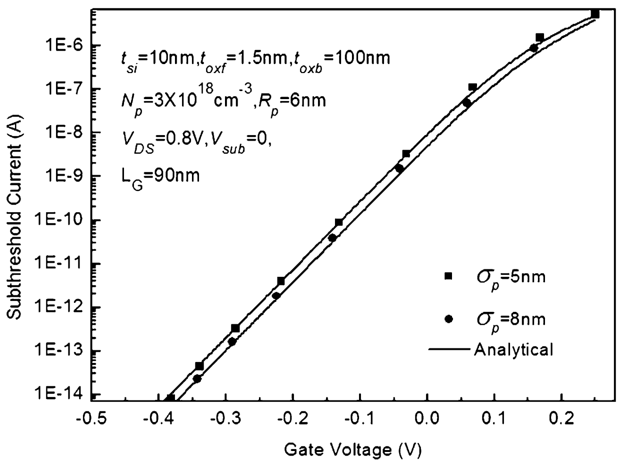

Fig. 3. Subthreshold current versus gate voltage for different σ_{p}.

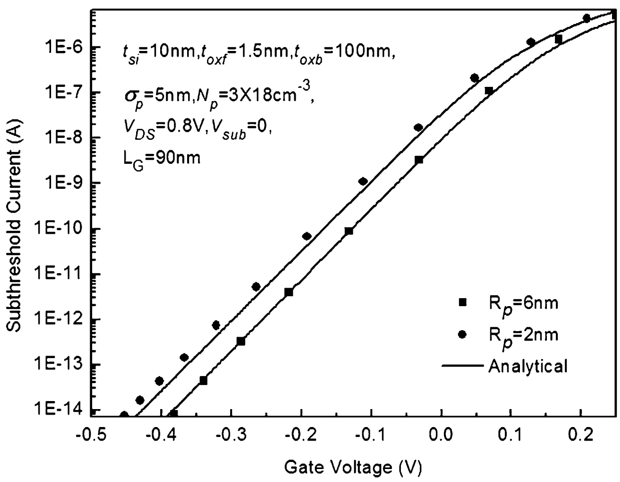

Fig. 4. Subthreshold current versus gate voltage for different R_{p}.

© 2012 The Japan Society of Applied Physics

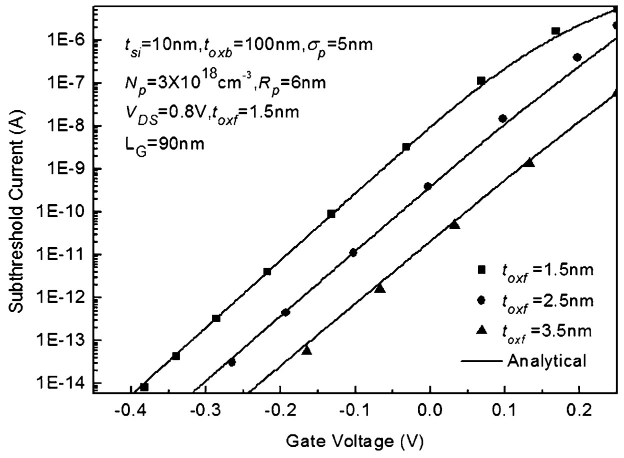

Fig. 5. Subthreshold current versus gate voltage for different t_{oxf}.

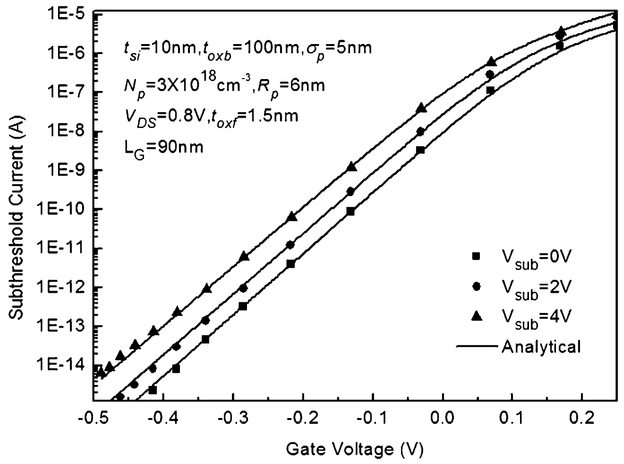

Fig. 6. Subthreshold current versus gate voltage for different V_{sub}.

can see that as the substrate voltage enhances, the total subthreshold current also increases because the back surface current increased. The results of our model agree with those of the numerical simulation, which shows the validity of the proposed analytical model. So with some moditication, the model can be used for double gate MOSFET.

4. Conclusion

Based on the surface potential function derived for an FD SOI MOSFET with vertical Gaussian doping profile, an analytical subthreshold current model is presented here. Both the diffusion current and the drift current are considered according to the Boltzmann transport equation. The front and the back channel currents are effectively derived through an inversion layer model which is accounted for the non-uniform doping profile. The model has been verified by the Sentaurus TCAD numerical simulation results with different parameters and agrees well with simulated results. According to the model calculations and the TCAD numerical simulation results, the derivations of the doping concentrations affect the subthreshold current significantly. The model can provide a deep physical insight and understanding of FD-SOI MOSFETs with a non-uniform doping profile operating in the subthreshold regime.

Acknowledgments

This work was supported by Specialized Research Fund for the Doctoral Program of Higher Education, the Ministry of Education, China (20090201120026) and the National Natural Science Foundation of China (61176038 and 61006033).

1) T. Sato, H. Ueyama, N. Nakayama, and K. Masu: IEEE J. Solid-State Circuits **44** (2009) 2977.
2) D. Bol, R. Ambroise, D. Flandre, and J.-D. Legat: Proc. IEEE Int. SOI Conf., 2008, p. 57.
3) T.-K. Chiang: Jpn. J. Appl. Phys. **47** (2008) 8297.
4) S. Pidin and M. Koyanagi: Jpn. J. Appl. Phys. **37** (1998) 1264.
5) R. Huang, Y. Wang, and R. Han: IEDM Tech. Dig., 1998, p. 118.
6) T. C. Hsiao and J. C. S. Woo: IEEE Trans. Electron Devices **42** (1995) 1120.
7) G. Zhang, Z. Shao, and K. Zhou: IEEE Trans. Electron Devices **55** (2008) 803.
8) P. K. Tiwari and S. Jit: J. Semicond. Technol. Sci. **10** (2010) 107.
9) S. Dubey, P. K. Tiwari, and S. Jit: J. Appl. Phys. **108** (2010) 034518.
10) P. Roy, B. Syamal, N. Mohankumar, and C. K. Sarkar: IEEE Int. Conf. Emerging Trends in Electronic and Photonic Devices and Systems, 2009, p. 70.
11) K. Suzuki, Y. Kataoka, S. Nagayama, C. W. Magee, T. H. Buyuklimanli, and T. Nagayama: IEEE Trans. Electron Devices **54** (2007) 262.
12) X.-L. Xu, R. Widenhofer, Y. Yu, O. Zia, S. Pozder, D. Hall, M. Rashed, D. Chang, S. Jallepalli, D. Connelly, T. V. Gompel, M. Olivares, M. Mendicino, J. Candelaria, S. Veeraraghavan, and D. Dow: Proc. 1999 IEEE Int. SOI Conf., p. 90.
13) J. Xu and M. C. Cheng: Proc. 2000 3rd IEEE Int. Caracas Conf. Devices, Circuits Syst., D29/1.
14) F. X. Yu, M. C. Cheng, and J. Xu: Proc. 2001 Int. Semicond. Device Research Symp., p. 613.
15) D. R. Poole and D. L. Kwong: IEEE Electron Device Lett. **7** (1986) 340.
16) P. A. Stolk, F. P. Widdershoven, and D. B. M. Klaassen: IEEE Trans. Electron Devices **45** (1998) 1960.

© 2012 The Japan Society of Applied Physics